Proceedings of the ECCOMAS Thematic International Conference on Simulation and Modeling of Biological Flows (SIMBIO 2011)
September 21–23, 2011, VUB, Brussels, Belgium

Impact of the mesh on the accuracy and efficiency of cardiovascular simulations.

E. Sauvage[*], C. Geuzaine[†], J.F. Remacle[*] and E. Marchandise [*]

1 Catholic University of Louvain-la-Neuve
Avenue Georges Lemaître, 4, B-1348 Louvain-la-Neuve, Belgium, {emilie.sauvage, jean-francois.remacle, emilie.marchandise}@uclouvain.be

2 University of Liège
Dept. of Electrical Engineering and Computer Science, Montefiore Institute B28, B-4000 Liège, Belgium, cgeuzaine@ulg.ac.be

Abstract

Mesh generation can be of great influence on the accuracy and efficiency of complex fluid simulations. In the present work, the effect of different surface meshing strategies is studied. Besides a standard uniform isotropic surface triangulation, a curvature field is computed on a realistic bypass anastomosis, which is then used to create curvature-adapted isotropic and anisotropic surface meshes. In addition, other mesh adaptation criteria suitable for biomedical applications, such as the distance from the centerline of the geometry, are considered. After meshing the inside volume of the model, an unsteady 3D fluid simulation is performed. The effect of the surface mesh on the resulting Wall Shear Stress demonstrates the adavantage of using the surface curvature map, especially in combination with anisotropic meshes.

Keywords: surface mesh adaptation, surface curvature, anisotropic mesh, bypass anastomosis, wall shear stress, computational fluid dynamics

Introduction

In the cardio-vascular field, atherosclerosis appears as one of the major diseases responsible for high death rate among elderly people. It manifests itself through arterial wall thicknening due to fat material deposition. This mechanism is also referred to as intimal hyperplasia. As the patient grows old, the arteries are progressively calcified, and the lumen undergoes a transformation from partially occluded (stenosis) to totally occluded situation. A direct consequence of this occlusion is a severely reduced amount of blood delivered to the limb members.

Many studies have pointed out material mismatch and hemodynamics as predominant factors in the disease development [13, 19, 21, 26]. Flow disturbances, wall shear stress, oscillatory shear stress play an important role in the localisation of intimal hyperplasia. A widely used treatment to counter the effects of the disease is to use bypass to sidestep the stenosed area of the arterial tree. Bypasses exist in many configurations involving different geometries and materials, and can be sewed to the artery in different ways [26]. One of them, the End-to-Side configuration (figure 1) is often employed for bypasses in the lower members of the body. In this configuration, the bypassing conduit is sewed upstream the stenosed part to the artery at the proximal anastomosis and downstream at the distal anastomosis. Unfortunately, statistics show high rate of bypass failure [4, 10, 27] despite many technical im-

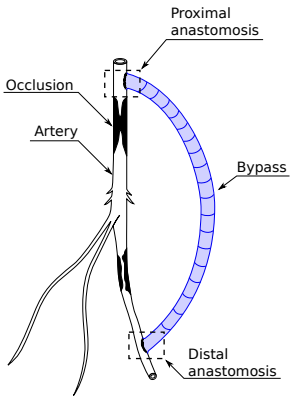

Figure 1 End-to-Side configuration of a bypass

provements. Material mismatch and geometrical configuration are thought to be the main causes of the progression of the disease. Although the mechanisms for bypass obstruction are not fully understood, studies have shown that atherosclerostic lesions appear in preferential sites. Typically, the lower (distal) anastomosis is an area where intimal hyperplasia seems to occur primarily [6, 7]. More precisely the heel, the toe and the floor region of the distal anastomosis are the most exposed [5, 8, 21].

The flow behaviour in the bypass-artery junction is subject to various numerical studies in the literature. Different approaches have been studied: 1D modelling, 3D fluid simulation, 3D fluid and structure simulation. The more complex the approach, the more computational time is necessary to obtain accurate results. Reducing the number of degrees of freedom, while keeping a high quality mesh, becomes an essential feature for numerical simulation.

To decrease the number of mesh vertices, the surface triangulation can be adapted to different criteria such as the distance from the arterial wall to the centerline or the curvature of the wall. The first criterion will lead to enhanced computational accuracy at low diameter vessels. Moreover, adding more vertices to the mesh in a transition area from large to small diameter is necessary for the surface mesh to follow more closely the shape of the real geometry. Consequently, large diameter regions are meshed with coarser elements. Adaptation according to the second criterion allows to account for the tortuosity of the geometry, which can be significant for real arteries.

In the following sections of this paper we introduce the different meshing procedures considered in the study: starting from isotropic surface meshes adapted according to either the distance map or the curvature map, the procedure is extended to anisotropic surface meshes. Afterwards, fluid simulations are presented to compare the quality of each mesh based on the evaluation of the wall shear stress.

Meshing procedure

Before generating a mesh suitable for numerical simulation, a surface reconstruction from original MRI images is performed. From the stack of medical images, a first mesh based on the stereolithographic format (STL) is obtained with the VMTK-Toolkit [34] implemented in the open source software Slicer3D [28, 29]. The outcome of the segmentation procedure is a mesh of the inner lumen surface of the artery. Since this triangulation is usually of low quality (poorly shaped elements) it is afterwards remeshed with Gmsh using surface parametrization [16, 31].

Surface parametrization

The input 3D surface mesh is partitioned into different patches of zero genus. The number of patches for a given geometry is such that every partition has a correct topology and a moderate aspect ratio between the smallest and the biggest length. Each of the patches present in the initial 3D geometry is first re-parametrized as a 2D plane surface. Two procedures can be used at this point: the harmonic algorithm which will map the mesh onto a unit circle, as presented in [31] or the conformal algorithm. The conformal algorithm can be advantageous because it preserves the angles, therefore the mapping is less distorted as shown in the figure 2. The mesh quality is shown to be superior to the harmonic algorithm [24]. Afterwards the patches

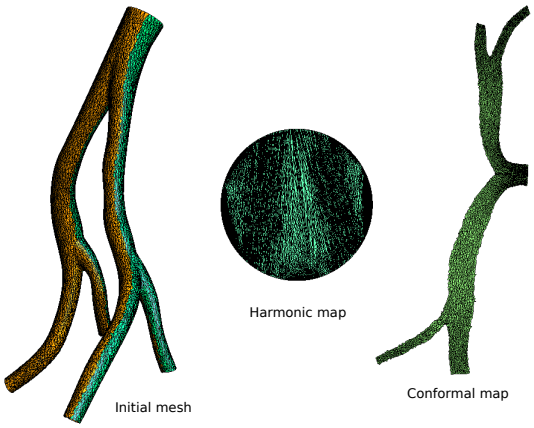

Figure 2 Parametrization of a blood vesssel surface with harmonic and conformal algorithm [24]

are remeshed separately using a standard 2D mesh generation algorithm (Delaunay, Frontal, etc). The remeshing can be done either with a constant mesh size field or with a field adapted to the distance from the centerline or to the curvature of the geometry as explained hereafter. Once the patches are remeshed, they can be easily mapped back thanks to the parametrization and reshape the original 3D geometry (figure 3).

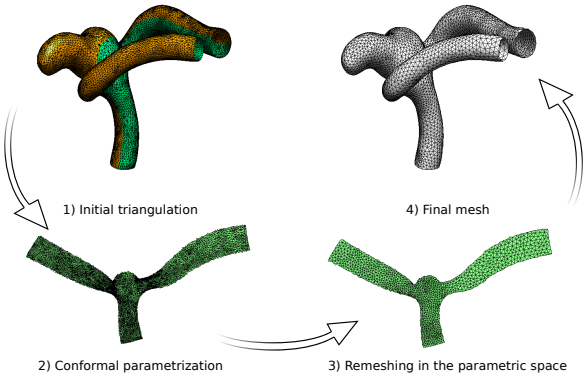

Figure 3 Remeshing procedure of an STL surface mesh [24]

Distance map

The distance map is a computed field containing information about the distance between the centerline and the inner surface of the vessel. The centerline of the artery used to establish this map is generated by the open source software VMTK [34]. The algorithm in VMTK is based on

a Voronoi tesselation which maximizes the radius of the spheres inscribed in the vessel along the path. The centers of those spheres define the points through which the centerline is passing. Once the centerline is determined, the distance map is obtained as the minimum Euclidean distance between the centerline and the surface. The purpose of the distance map is twofold. First, it serves as a means of controlling the characterictic element size according to the vessel diameter. (The grid characterictic length is directly proportional to the vessel diameter.) Second, it can be used to extrude a layer of cells at the surface whose thickness is a function of the vessel diameter.

Curvature map

The curvature map is a field derived form the normals of the surface and measures its local radius at each point. Before introducing the curvature algorithm, let us define some basic geometrical concepts.

Let $\mathbf{S}$ be a triangulated surface, and $\mathbf{P}$ one of its vertices. The vectors noted $\mathbf{n}$ and $\mathbf{t}$ are respectively the normal and the tangent vector originating from $\mathbf{P}$. By definition, the normal curvature κ_n, at point $\mathbf{P}$ is the reciprocal of the radius of the osculating circle that best approximates the planar curve resulting from the intersection of a plane passing by $\mathbf{P}$ with the surface $\mathbf{S}$. There exists a multitude of planar curves, therefore a mutlitude of normal curvatures κ_n can be defined at point $\mathbf{P}$.

From all the possible normal curvatures, the minimal normal curvature κ_1 and the maximal normal curvature κ_2 are called the principal curvatures. The associated vectors $\mathbf{t_1}$ and $\mathbf{t_2}$ lying in the tangent plane through point $\mathbf{P}$ are called the principal directions.

One way to find the principal curvatures is to rotate the local coordinate system so that the Weingarten curvature matrix $\mathbf{W}$ (also known as the second fundamental tensor $\mathbf{II}$) becomes diagonal. This matrix measures the directional derivative of the normal i.e. $\mathbf{Wt} = \frac{\partial \mathbf{n}}{\partial \mathbf{t}}$, where $\mathbf{n}$ is the normal vector of the plane tangent to the surface $\mathbf{S}$ passing by $\mathbf{P}$.

Expressed in a local coordinate system defined by the principal directions $\mathbf{t_1}$ and $\mathbf{t_2}$, $\mathbf{W}$ becomes a diagonal matrix of the form:

$$\mathbf{W} = [\mathbf{t}_1\mathbf{t}_2] \begin{bmatrix} \kappa_1 & 0 \\ 0 & \kappa_2 \end{bmatrix} [\mathbf{t}_1\mathbf{t}_2]^{-1}$$

The curvature tensor, noted $\mathbf{T}$, which measures the change of the normal with respect to a tangent vector at each mesh vertex $\mathbf{P}$, is expressed as a symmetric 3×3 matrix with eigenvalues κ_1, κ_2 and 0 and the corresponding eigenvectors $\mathbf{t}_1$, $\mathbf{t}_2$, $\mathbf{n}$:

$$\mathbf{T} = \mathbf{PDP}^{-1}$$

with $\mathbf{P} = [\mathbf{t_1}, \mathbf{t_2}, \mathbf{n}]$ and $\mathbf{D} = diag(\kappa_1, \kappa_2, 0)$.

Different methods have been proposed in the literature to compute the surface normal curvature. They can be classified in three main categories:

- Patch fitting methods, which attempt to fit a smooth polynomial surface through each mesh vertex P and its neighbors. The local curvature can be deducted from the coefficient used in the polynomial fit. Such methods are used in [15, 30]

- Normal-based estimation of the curvature, which is a class of methods originally proposed in [35]. It starts with the approximation of normal curvature along the edges of the surface elements using the following formula:

  $$\kappa_{ij} = 2\frac{(\mathbf{p}_j - \mathbf{p}_i)\mathbf{n}_i}{\|\mathbf{p}_j - \mathbf{p}_i\|^2},$$

  where i and j are the indexes of the edge vertices, $\mathbf{p}_i$, $\mathbf{p}_j$ denote the vertex positions and $\mathbf{n}_i$ is the normal at vertex i. The principal curvatures can be expressed as a function of the eigenvalues of a symmetric matrix [25] or can be obtained as a solution of a least-squares minimization [2, 15].

- The last category of methods establishes a parametrization on the discrete surface and computes the curvature from the derivatives of this parametrization.

The method used in this paper belongs to the third category and was originally proposed by S. Rusinkiewicz [32]. It first computes the curvature per triangular element of the mesh, then estimates the curvature per vertex by weighted average of the direct neighboring elements. The algorithm starts with the per-face curvature computation, in which the second fundamental tensor $\mathbf{II}$ introduced earlier is expressed in terms of derivatives of the surface normal. The multiplication of this tensor by a vector $\mathbf{s} = (s_1, s_2)$ belonging to a tangent plane of the surface will give the derivatives of the normal in the direction of $\mathbf{s}$.

In the Rusinkiewicz approach, the curvature tensor $\mathbf{T}$ can be seen as a quantification of the change of the normal field at P projected on the plane tangent to the surface S. The estimation of the derivatives of the normals $D_s n$, per face, is done via a finite difference approach. The idea is to use the edges (e_0, e_1, e_2) of a triangle as 3 tangent directions in which the derivatives will be approximated, as follows, by the difference of the normals in the 2 vertices of each edge (see figure 4).

$$\mathbf{II} \begin{pmatrix} e_0 \cdot u \\ e_0 \cdot v \end{pmatrix} = \begin{pmatrix} (n_2 - n_1) \cdot u \\ (n_2 - n_1) \cdot v \end{pmatrix}$$
$$\mathbf{II} \begin{pmatrix} e_1 \cdot u \\ e_1 \cdot v \end{pmatrix} = \begin{pmatrix} (n_0 - n_2) \cdot u \\ (n_0 - n_2) \cdot v \end{pmatrix}$$
$$\mathbf{II} \begin{pmatrix} e_2 \cdot u \\ e_2 \cdot v \end{pmatrix} = \begin{pmatrix} (n_1 - n_0) \cdot u \\ (n_1 - n_0) \cdot v \end{pmatrix}$$

This is a system of linear constraints for the upper triangle of the symmetric tensor $\mathbf{II}$, which is solved in least squares sense.

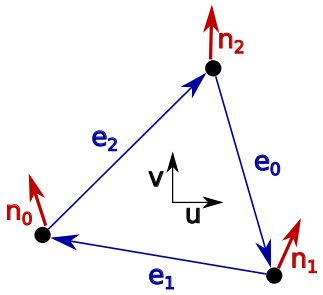

Figure 4 Notation for the local element edges and normals in the algorithm of Rusinkiewicz

Once the values κ_1 and κ_2 are computed, the element characteristic length is determined as

$$\mathrm{cl}_e = \frac{2\pi}{|\kappa_{mean}|N},$$

where N is a user-defined number of mesh points on imaginary osculation circle at given surface point and

$$\kappa_{mean} = \frac{\kappa_1 + \kappa_2}{2}$$

is the mean curvature.

Anisotropic surface mesh adapted on the curvature

The anisotropic surface mesh is generated by an external library BAMG, developed by F. Hecht [20] and linked to Gmsh. To perform the meshing operation, a discrete metric map is designed and used as input for BAMG. The map is supplied by the user, and in the present study, the curvature map is chosen to be the input metric map.

At each vertex of the surface mesh is defined a metric tensor given under the general form:

$$\mathbf{M} = \mathbf{P}\tilde{\mathbf{\Lambda}}\mathbf{P}^{-1}, \text{ with } \tilde{\mathbf{\Lambda}} = \begin{pmatrix} \tilde{\lambda_1} & 0 & 0 \\ 0 & \tilde{\lambda_2} & 0 \\ 0 & 0 & \tilde{\lambda_3} \end{pmatrix},$$
$$\mathbf{P} = [\mathbf{t_1}, \mathbf{t_2}, \mathbf{n}]$$
$$\text{and } \tilde{\lambda_i} = \mathrm{f}(\kappa_i, \mathrm{h}_{max}, \mathrm{h}_{min})$$

where $\mathbf{P}$ is the matrix whose columns are the principal curvature directions, and κ_i are the eigenvalues of the curvature tensor $\mathbf{T}$. The metric tensor defined by this relation is anisotropic by nature. The principal directions are given by the eigenvectors matrix $\mathbf{P}$ and the associated element sizes are prescribed by the coefficients $\tilde{\lambda_i}$. The parameters h_{max} and h_{min} represent the maximal and the minimal element size allowed in the mesh. Those bounds are introduced to avoid problems such as infinite size elements that may occur in case of zero eigenvalues. See [12, 14] for further details.

Volume mesh

Each surface triangulation, adapted or not based on the curvature/distance criterion, is meshed in volume. The volume mesh generation is performed in two steps. The first consists in an inward extrusion of a boundary layer in the fluid region at the wall. The second step produces the mesh of the remaining volume inside the vessel. The resulting mesh of those two operations is shown in Figure 5.

The purpose of the boundary layer meshing is to enhance

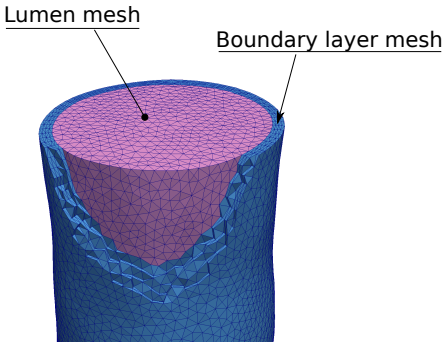

Figure 5 Volume mesh of the blood vessel with boundary layer

the resolution of wall quantities, such as the wall shear stress (WSS). Several studies [3, 33, 36] relate the great improvement given by the refined layer at the wall in the WSS determination.

The extrusion used in this study is made of 4 layers of cells extruded along a direction perpendicular to the wall towards the inside of the fluid domain. For one extruded layer, prisms are generated (one triangular face of every prisms lies on the surface mesh), then subdivided into tetrahedra. The resulting mesh is uniquely made of tetrahedra and the extrusion procedure allows a systematic and regular arrangement of the elements in the boundary layer.

Thanks to the distance map from the centerline, the tickness of the boundary layer (10 % of the radius) varies accordingely with the diameter.

For the rest of the volume (left after the boundary layer extrusion) a standard mesh algorithm (Delaunay or Frontal) is used to cover the vessel lumen.

Flow Simulations

To demonstrate the effect of mesh adaptation on the surface, fluid simulations are run on the geometry of a distal anastomosis (figure 6). The comparison of the results is based on the WSS.

Initial Surface meshes

The extracted surface of the distal anaostomose from the medical images is remeshed by four different triangulations (figure 7). The first one is a uniform mesh (figure 7(a)). The second mesh is based on the distance map and implies a mesh refinement at places where the diameter of the vessel is smaller. For this particular geometry, the occluded artery has a higher node density. Everywhere else, the characterictic element size of this “distance mesh” is fairly constant (figure 7(b)). The third (figure 7(c)) and the

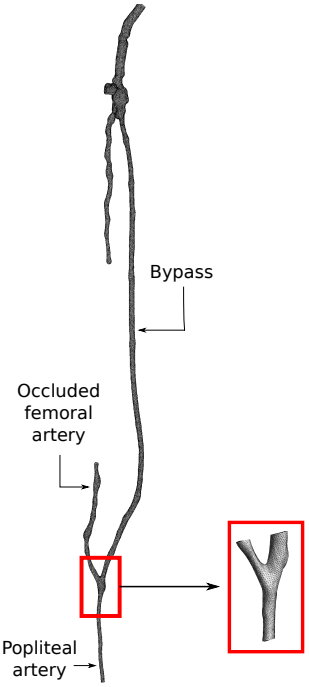

Figure 6 Distal anatomosis extracted from a femoropopliteal bypass

fourth mesh (figure 7(d)) use the curvature map for refinement. The main difference between the last two meshes lies in the fact that the former is isotropic, whereas the latter is anisotropic and takes into account not only the values of curvature values, but also its principal directions.

To ensure a fair comparison of the simulation results, the number of nodes on the surface is approximately the same. Table 1 summarizes the node and element count for each mesh.

Mesh type	Nb. elements on the surface	Total nb of nodes	Total nb. of elements
Uniform mesh	28113	87216	482093
Distance mesh	28328	84645	469577
Isotropic mesh curvature	28289	86312	477954
Anisotropic mesh curvature	28280	84826	468498

Table 1 Nodes and elements number on the surface and inside the whole volume

Simulation set-up

Prior to the MRI scan, a series of Echo Doppler measurements has been realized on the same patient (figure 8). The average flux over a cardiac cycle taken upstream (in the bypass) and downstream (in the popliteal artery) from the Echo Doppler will be used to establish the inlet and outlet boundary conditions of the model. As shown in fig. 6, the ending part of the bypass (above the anastomosis) is taken as inlet of the model, and the popliteal artery is used for

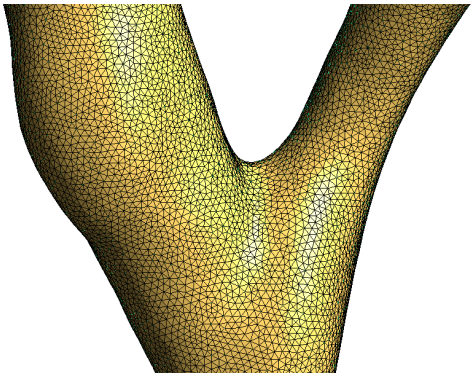

(a) Uniform mesh

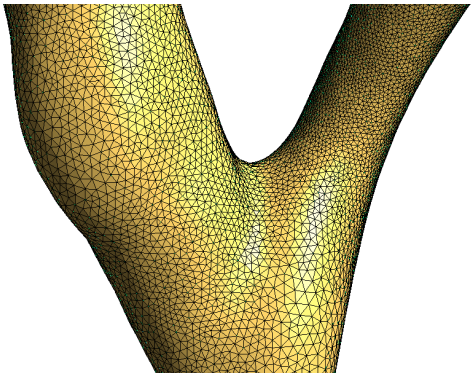

(b) Distance mesh

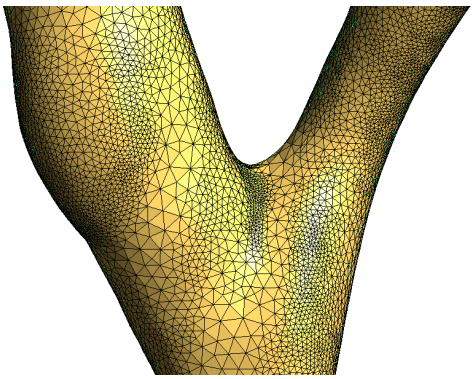

(c) Isotropic surface mesh based on curvature

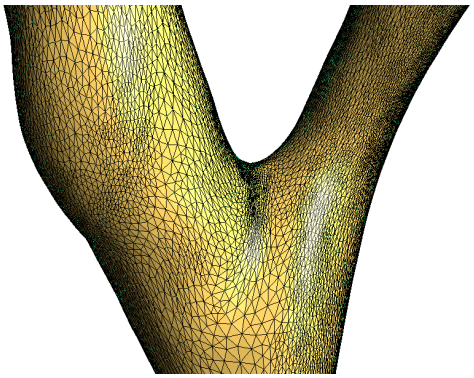

(d) Anisotropic surface mesh based on curvature

Figure 7 Initial surface meshes

the outlet. Dirichlet conditions for velocity are prescribed for the two surfaces. At the blocked femoral artery, a zero Neumann condition for velocity is imposed to preserve the well-posedness of the problem.

To avoid singularities at the edges of the inlet and outlet surfaces, a parabolic velocity profile is imposed. The inlet/outlet velocity profiles are deduced from the average flux data, by multiplying by a shape coefficient $\left(1 - \frac{r^2}{R^2}\right)$ and dividing its norm over the section area. The parameters r and R are respectively the local radial position and the radius of the surface.

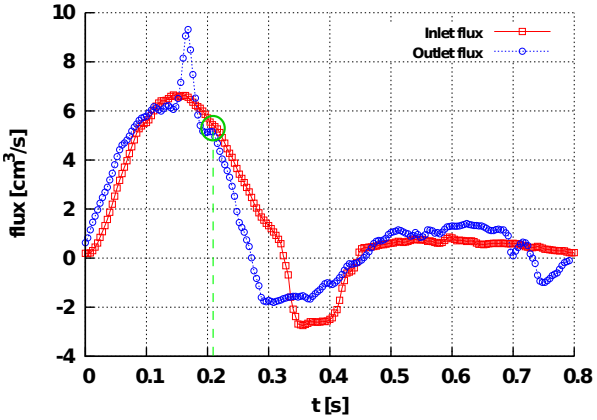

Figure 8 Inlet and outlet fluxes of the distal anastomosis measured by the EchoDoppler. The green circle at 0.21s indicates the time used for the post-treatment of the WSS data.

To solve the 3D fluid problem of the blood flow passing through the anastomosis, the solver LifeV [1, 9] has been employed. LifeV uses Finite Element Method to discretize the Oseen equations as a model for viscous and incompressible fluid at low Reynolds number.

Numerical results

The role of wall shear stress parameter in the development of the atherosclerostic disease is not fully understood yet. Several studies in the past [17, 22, 23] have pointed out that for arterial system, intimal hyperplasia deposition occurs mainly in regions of low WSS. However, WSS might not be the only parameter to determine plaque deposition [22]. Oscillatory Shear Index and Wall Shear Stress Gradient can also be good indicators.

In the case of distal graft junction, research studies [8, 11, 18, 23] have shown that the regions where intimal thickening preferably developed are the heel, the toe and the floor regions of the anastomosis. Depending on the geometry, those regions might or might not be associated with low WSS. In the present paper, the WSS is studied along a closed contour at two different sections (figure 9). The location of the first contour (ring Nr1) is such that it sits on the line joining the heel and the toe of the anastomosis. For this geometry, the toe is harder to locate because of the very smooth transition from the graft to the artery. The

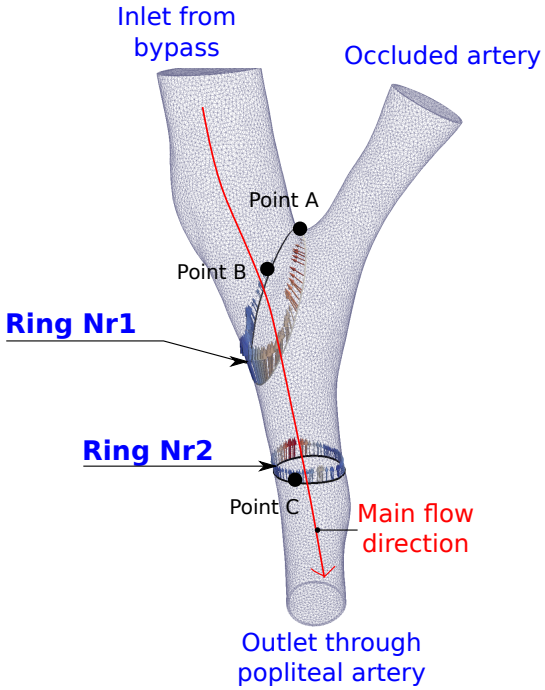

Figure 9 Location of the three different contours on which the WSS vector are computed

second contour (ring Nr2) has been selected on a relatively straight part of the popliteal artery in order to compare the resolution of the different meshes also in a region not critical for the disease development.

The wall shear stress vector is computed according to the following formulas:

$$\boldsymbol{\tau} = \mathbf{t}_s = \mathbf{t} - (\mathbf{t} \cdot \mathbf{n}_s)\mathbf{n}_s \tag{1}$$

where $\mathbf{t}$ is the traction vector defined as:

$$\mathbf{t} = \sigma \mathbf{n}_s = \left[-p\mathbb{I} + \mu(\nabla \mathbf{u} + \nabla \mathbf{u}^T) \right] \mathbf{n}_s \tag{2}$$

σ is the stress tensor, $\mathbf{n}_s$ is the normal vector to the surface at a point of the contour and p and $\mathbf{u}$ are respectively the pressure and the velocity vector at that point.

If plotting the isolines of WSS (figure 10), the heel of the anastomosis seems to be at a location of high spatial shear stress gradient as observed in [18]. In order to study

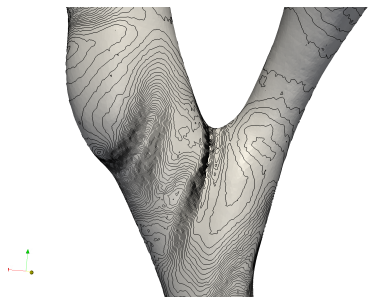

Figure 10 Isolines of WSS

the WSS dependence on the characteristic length scale of

the mesh, a fluid simulation has been performed on four uniform meshes with increasing number of nodes. The total number of triangular elements in the volume mesh varies from approximately 4.8×10^5 to 5.5×10^6. As the characteristic length of the mesh decreases, the range of wall shear stress values stabilizes (figure 11), i.e. the values converge, overall, to a limit as the number of nodes increases.

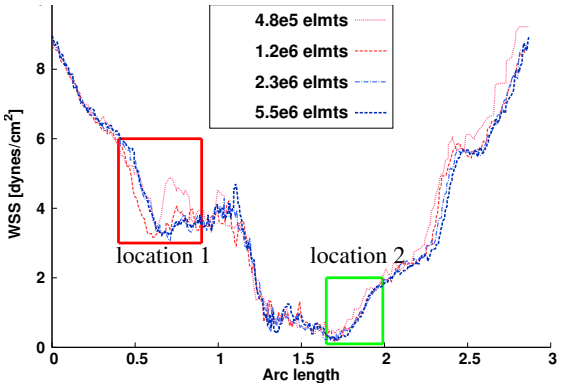

(a) WSS along the whole contour

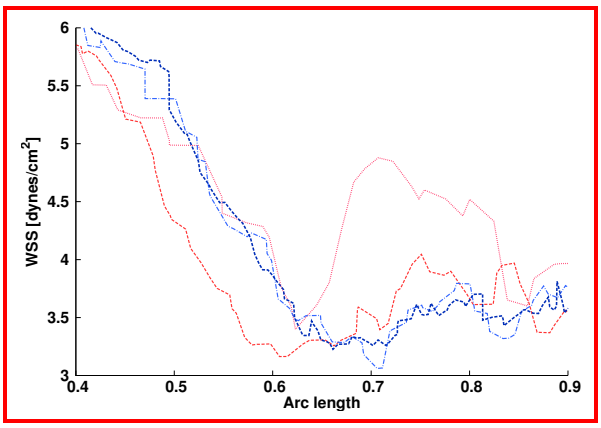

(b) WSS detailed view at location 1

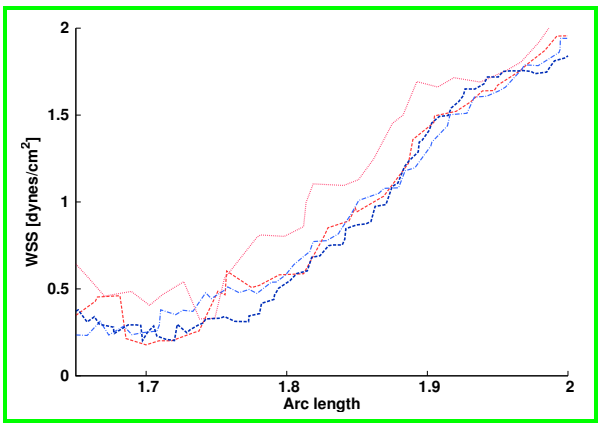

(c) WSS detailed view at location 2

Figure 11 WSS plotted along the ring Nr1 for isotropic uniform meshes of increasing number of element in volume

The finest of the uniform meshes is taken as a reference for the comparison with the four original meshes: uniform, adapted with respect to distance, isotropic and anisotropic curvature-based surface meshes. The relative difference of the WSS value between these four meshes and the reference mesh is computed at a point where WSS attains its minimum. The percentage of the relative difference is shown in the following charts for the two rings.

Refinement using the curvature criteria seems to be advantageous while dealing with vessels of multiple branches connection (typically an anastomosis) or tortuous geometry. For the present geometry, the curvature mesh adaptation allows to refine at the heel (point A) of the anastomosis which is one of the zones susceptible to develop intimal thickening. In this area, the anisotropic mesh adaptation results yields the smallest deviation of WSS (figure 12) from the reference mesh.

However, at point B of the first ring (fig. 9), the description of the WSS by the anisotropic and isotropic mesh based on curvature is fairly poor. Figure 13 shows how large is the relative difference: 31.97% and 44.40%, respectively. This is due to the fact that around point B the surface is relatively flat, therefore the curvature remeshing algorithm does not consider it a refinement target area.

The second ring in figure 14 shows results similar to ring Nr1: the anisotropic mesh based on surface curvature again exhibits the smallest relative difference compared to the reference mesh. At the location of the second ring, the geometry is quasi cylindrical, which means that one of the curvature principal directions is approximately parallel to the centerline of the vessel, while the other is tangential to its surface and perpendicular to the centerline. The mesh cells produced by the anisotropical algorithm are well aligned with the direction of the flow, which results in more accurate velocity as well as the WSS computation.

When the geometry is mainly cylindrical (no splitting in several branches) the isotropic adaptation based on curvature and on distance from the centerline gives similar results. For relatively straight vessels, the two criteria are connected. As the diameter of the vessel decreases, both the distance from the centerline and the mean curvature decrease the mesh characteristic length. In case of complex cardiovascular geometry, these two criteria can indicate mesh adaptation in very different locations.

Conclusions

Surface remeshing with local refinement based on curvature produces quality meshes suitable for blood flow simulations. Since the adaptation criteria is purely geometry-based, the flow field is not required a priori to obtain an initial metric. The principal curvature directions on vessel surface can serve as input for the anisotropic mesh generator. In agreement with literature, the anisotropic mesh produces the most accurate results which are comparable to data obtained on a uniform mesh with several times more degrees of freedom. The meshes inside the vessel volume used in this paper are isotropic. In the future, 3D anisotropic dynamic adaptation will be implemented in Gmsh to further improve the efficiency of the numerical simulation. Both curvature and distance from centerline are constant on a cylindrical surface, there-

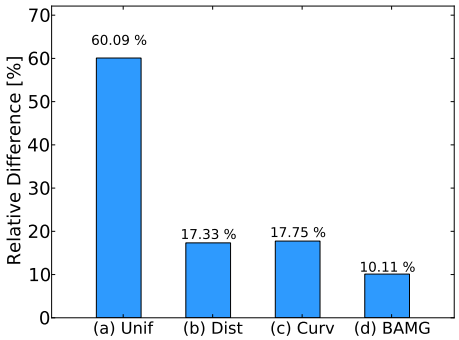

Figure 12 Relative difference in the minimum values of WSS of the 4 tested meshes with the finest uniform mesh on the ring Nr1. (a) uniform coarse mesh, (b) distance-adapted mesh (c) isotropic mesh adapted with respect to curvature (d) anisotropic mesh obtained with the library BAMG

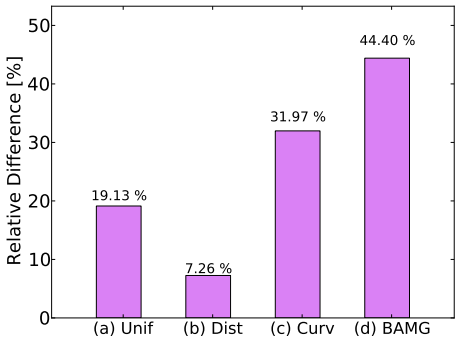

Figure 13 Relative difference in the values of WSS picked at Point B (ring Nr1) of the 4 tested meshes with the finest uniform mesh on the ring Nr1. (a) uniform coarse mesh, (b) distance-adapted mesh (c) isotropic mesh adapted with respect to curvature (d) anisotropic mesh obtained with the library BAMG

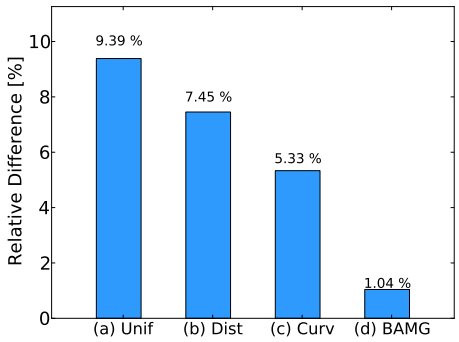

Figure 14 Relative difference in the minimum values of WSS between each of the 4 tested meshes and the finest uniform mesh on the ring Nr2. (a) uniform coarse mesh, (b) distance-adapted mesh (c) isotropic mesh adapted with respect to curvature (d) anisotropic mesh obtained with the library BAMG

fore the resulting meshes show very similar features. The advantages of each respective approach are more case-specific.

Acknowledgements

The first author thanks Paolo Crosetto and Claudia Colciago for their precious help with LifeV.

References

[1] Lifev project. `http://www.lifev.org`.

[2] Y. An, C. Shao, X. Wang, and Z. Li. Estimating principal curvatures and principal directions from discrete surfaces using discrete curve model. *Journal of Information and Computational Science*, 8:296–311, 2011.

[3] L. Antiga. *Patient-Specific Modeling of Geometry and Blood Flow in Large Arteries*. PhD thesis, Politecnico di Milano, 2002.

[4] A.Tura. *Vascular Grafts: Experiment and Modelling*, volume 1. WIT Press, first edition edition, 2003.

[5] H. Bassiouny, S. White, S. Glagov, E. Choi, D. Giddens, and C. Zarins. Anastomotic intimal hyperplasia: Mechanical injury or flow induced. *Journal of Vascular Surgery*, 15:708–716, 1992.

[6] E. Chignier, J. Guidollet, C. Lhopital, P. Louisot, and R. Eloy. Lipid accumulation in prosthetic vascular grafts: Experimental study. *American Journal of Pathology*, 137:531–540, 1990.

[7] A. Clowes, A. Gown, S. Hanson, and M. Reidy. Mechanisms of arterial graft failure: 1. role of cellular proliferation in early healing of ptfe protheses. *American Journal of Pathology*, 118:43–54, 1985.

[8] J. Cole, J. Watterson, and M. O'Reilly. Blood flow characteristics in a femoral artery bypass graft. *Developments in Chemical Engineering and Mineral Processing*, 11:15–28, 2003.

[9] P. Crosetto, S. Deparis, G. Fourestey, and A. Quarteroni. Parallel algorithms for fluid-structure interaction problems in haemodynamics. *Siam Journal on Scientific Computing*, 33:1598–1622, 2011.

[10] H. V. Damme, M. Deprez, E. Creemers, and R. Limet. Intinsic structural failure of polyester (dacron) vascular grafts: a general review. *Acta Chirurgica Belgica*, 105:249–255, 2005.

[11] H. Do, A. A. Owida, W. Yang, and Y. Morsi. Numerical simulation of the hemodynamics in end-to-side anstomoses. *International Journal For Numerical Methods in Fluids*, 2010.

[12] M. C. Dıaz and F. Hecht. Curvature estimation for unstructured triangulations of surfaces. Technical Report 2672, Institut National de Recherche en Informatique et en Automatique, 1995.

[13] C. Ethier, S. Prakash, D. Steinman, R. Leask, G. Couch, and M. Ojha. Steady flow separation patterns in a 45 degree junction. *Journal of Fluid Mechanics*, 411:1–38, 2000.

[14] P. Frey and F. Alauzet. Anisotropic mesh adaptation

for cfd computations. *Computer methods in applied mechanics and engineering*, 194:5068–5082, 2005.

[15] R. V. Garimella and B. K. Swartz. Curvature estimation for unstructured triangulations of surfaces. Technical Report LA-UR-03-8240, Los Alamos National Laboratory, 2003.

[16] C. Geuzaine and J. Remacle. Gmsh: A three dimensional finite element mesh generator with built-in pre- and post-processing facilities. *International Journal for Numerical Methods in Engineering*, 79:1309–1331, 2009.

[17] C. Gibson, L. Diaz, K. Kandarpa, F. Sacks, R. Pasternak, T. Sandor, C. Feldman, and P. Stone. Relation of vessel wall shear stress to atherosclerosis progression in human coronary arteries. *Arteriosclerosis, Thrombosis and Vascular Biology*, 13:310–315, 1993.

[18] S. Giordana, S. Sherwin, J. Peiro, D. Doorly, J. Crane, K. Lee, N. Cheshire, and C. Caro. Local and global geometric influence on steady flow in distal anastomoses of peripheral bypass grafts. *Journal of Biomechanical Engineering*, 127:1087–1098, 2005.

[19] H. Haruguchi and S. Teraoka. Intimal hyperplasia and hemodynamic factors in arterial bypass and arteriovenous grafts: a review. *The Japanese Society for Artificial Organs*, 6:227–235, 2003.

[20] F. Hecht. Bamg: Bidimensional anisotropic mesh generator, 2006.

[21] R. Keynton, M. Evancho, R. Sims, N. Rodway, A. Gobin, and S. Rittgers. Intimal hyperplasia and wall shear in arterial bypass graft distal anastomoses: an in vivo model study. *Journal of Biomechanical Engineering*, 123:464–473, 2001.

[22] J. Knight, U. Olgac, S. Saur, D. Poulikakos, W. Marshall, P. Cattin, H.Alkadhi, and V. Kurtcuoglu. Choosing the optimal wall shear parameter for the prediction of plaque location. *Atherosclerosis*, 211:445–450, 2010.

[23] F. Loth, P. Fisher, and H. Bassiouny. Blood flow in end-to-side anastomoses. *Annual Review of Fluid Mechanics*, 40:367–393, 2008.

[24] E. Marchandise, P. Crosetto, C. Geuzaine, J. Remacle, and E. sauvage. Quality open source mesh generation for cardiovascular flow simulations. In *Springer Series on Modeling, Simulation and Applications*. Springer-Verlag, Berlin Heidelberg, 2011.

[25] E. Mathews, W. B. W, and M. Ritter. Implementation of an algorithm for approximating the curvature tensor on a triangular surface mesh in the vish environment. In *In 6th High-End Visualization Workshop, Obergurgl. Austria*, 2010.

[26] F. Migliavaca and G. Dubini. Computational modeling of vascular anastomoses. *Biomechanics and Modeling in Mechanobiology*, 3:235–250, 2005.

[27] V. M. Miller. Femoropopliteal bypass graft patency: An analysis of 156 cases. *Annals of Surgery*, 180:35–38, 1974.

[28] S. Pipper, M. Halle, and R. Kikinis. Slicer 3d. *Proceedings of the 1st IEEE International Symposium on Biomedical Imaging: From Nano to Macro*, pages 632–635, 2004.

[29] S. Pipper and R. Kikinis. 3dslicer a multi-platform, free and opensource software package for visualization and medical image computing. `http://www.slicer.org`, 2007.

[30] A. Razdan and M. Bae. Curvature estimation scheme for triangle meshes using biquadratic bézier patches. *Computer-Aided Design*, pages 1481–1491, 2005.

[31] J. Remacle, C. Geuzaine, G. Compere, and E. Marchandise. High quality surface remeshing using harmonic maps. *International Journal for Numerical Methods in Engineering*, 83:403–425, 2010.

[32] S. Rusinkiewicz. Estimating curvatures and their derivatives on triangle meshes. In *Symposium on 3D Data Processing, Visualization, and Transmission*, Sept. 2004.

[33] M. Shephard, K. Jansen, O. Sahni, and L. Diachin. Parallel adaptive simulations on unstructured meshes. In *Journal of Physics: Conference Series*, 2007.

[34] D. Steinman and L. Antiga. Vmtk - the vascular modelling toolkit. `http://www.vmtk.org`.

[35] G. Taubin. Estimating the tensor of curvature of a surface from a polyhedral approximation. *Computer Vision, IEEE International Conference on Computer Vision*, 1955.

[36] M. Zhou, O. Sahni, H. Kim, C. Figueroa, C. Taylor, M. Shephard, and K. Jansen. Cardiovascular flow simulation at extreme scale. *Computational Mechanics*, 46:71–82, 2010.